Destabilization of hidden order in URu2Si2 under magnetic field and pressure

William Knafo, S. Araki, G. Lapertot, D. Aoki, G. Knebel, D. Braithwaite

Squeezing out field-induced reentrant hidden-order in URu_2Si_2

W. Knafo[1], S. Araki[2], G. Lapertot[3], D. Aoki[3,4], G. Knebel[3], D. Braithwaite[3]

[1] *LNCMI, 143 Avenue de Rangueil, 31400 Toulouse, France*

[2] *Department of Physics, Okayama University, Okayama 700-8530, Japan*

[3] *Univ. Grenoble Alpes, CEA, IRIG, PHELIQS, F-38000 Grenoble, France*

[4] *Institute for Materials Research, Tohoku University, Ibaraki 311-1313, Japan*

e-mail: william.knafo@lncmi.cnrs.fr

February 24, 2020

16:02

The mystery of the hidden-order phase in the correlated-electron paramagnet URu_2Si_2 is still resisting after decades of experimental and theoretical efforts. To solve the problem, one strategy is to search for clues in the subtle competition between this state and neighboring magnetically-ordered states. It is now well-established that long-range magnetic order can be stabilized in this metal under pressure (antiferromagnetism) or magnetic field applied along the easy magnetic axis c (spin-density wave). However, the full boundaries of the hidden-order phase in the pressure-magnetic field plane have not been determined so far. Here, we present a systematic investigation of URu_2Si_2 under combined high pressures and intense magnetic fields. The boundaries of the hidden-order, antiferromagnetic and spin-density-wave phases are mapped out, indicating a rich and complex three-dimensional phase diagram. We show that the field-induced spin-density-wave and hidden-order phases disappear in favor of antiferromagnetism at high pressure. Interestingly, a large number of phase boundaries are controlled by the field- and pressure-dependences of a single parameter. These results constitute new constraints for theories aiming to model the electronic correlations and the ordered phases in URu_2Si_2.

Intense research on correlated-electrons quantum materials is focused on the competition between ordered and disordered electronic states, their tuning via quantum phase transitions and their possible relationship with unconventional superconductivity [1],[2],[3],[4],[5],[6]. Amongst these systems, URu_2Si_2 occupies a very special place, due to the unique richness of its quantum electronic properties and the challenge to understand them [7]. After now more than 30 years and hundreds of experimental and theoretical papers, discussions and controversies are still going on about the nature of the so-called 'hidden-order' (HO) phase, which is established below the temperature T_0 = 17.5 K. Efforts have been devoted to elucidate its order parameter, but none was successful to determine it unambiguously so far. The transition at T_0 is associated with strong physical responses, such as a large jump in the heat capacity [8], an enhancement and a sudden gapping of intersite magnetic fluctuations [9],[10], a boost of the carrier mobility and a modification of the Fermi surface [11],[12],[13],[14], and the opening of an electronic gap [15],[16]. While a small antiferromagnetic (AF) moment was observed below T_0 by neutron diffraction [17], ambient-pressure antiferromagnetism is now accepted to be an extrinsic property induced by crystal defects and distortions [18]. From Fermi surface studies under pressure, it has been proposed that the HO has the same periodicity of wavevector $\mathbf{k}_0$ = (0 0 1) than the AF phase stabilized under pressure [19]. The symmetry of the HO has also been considered: following torque [20] and diffraction [21] experiments, a nematic behavior in the HO phase has been proposed. However, this picture faces now a series of contradictory diffraction [22],[23], NMR [24], and thermodynamic [25] experiments and the question of the symmetry remains open. Beyond experiments, many theories were proposed to describe the HO within different approaches: localized, itinerant, or dual (localized/itinerant) *f*-electrons, multipolar order, nematicity, spin liquid, 'hastatic' order, etc. [26],[27],[28],[29],[30]. A difficulty is to evidence experimentally, in a direct and unambiguous manner, the order parameters proposed by these models.

To reveal the physics of the hidden order, an alternative route is to study how it can be destabilized by tuning external parameters [5]. In the HO state, gapped low-energy magnetic fluctuations peaked at the wavevectors $\mathbf{k_0}$ and $\mathbf{k_1}$ = (0.6 0 0) [9],[10] can be seen as precursors of long-range magnetic ordering with the same wavevectors and indicate nearby

quantum phase transitions. In heavy-fermion paramagnets, such intersite magnetic fluctuations often indicate the proximity of a magnetically-ordered phase. For instance, in the textbook $CeRu_2Si_2$ case quantum magnetic fluctuations with wavevector $\mathbf{k_1}$ = (0.31 0 0) can be transformed into long-range magnetic order with the same wavevector by La-doping [31]. As well as doping, pressure and magnetic field are ideal tools to tune the electronic interactions. In URu_2Si_2, hydrostatic pressure [32],[33],[34] (but also uniaxial strain [35], and doping with Rh or Fe [36],[37]) leads to a phase transition from the HO phase towards an AF state, with the wavevector $\mathbf{k_0}$ and the moments aligned along the **c**-axis of the tetragonal crystal. At ambient pressure, under a magnetic field from 35 to 39 T applied along **c**, the hidden order is replaced by a spin-density wave (SDW), where the magnetic moments are ordered with the wavevector $\mathbf{k_1}$ and aligned along **c** [38],[39]. Remarkably, experiments under combined magnetic field and pressure, in the limited ranges 16 T / 2 GPa [40], and 45 T / 1 GPa [41], showed that a magnetic field applied to the pressure-induced AF phase induces a return into the HO phase [40], and that the SDW phase shrinks and moves to higher fields under pressure [41]. The relative stability of these different types of order is clearly complex, and a full description of how URu_2Si_2 evolves under combined pressure and magnetic field is needed.

Here, we benefited from the recent development of a specifically designed anvil-type cell for pulsed magnetic fields [42],[43] to extract the three-dimensional (3D) magnetic field – pressure – temperature phase diagram of URu_2Si_2. Its magnetoresistivity was measured in magnetic fields up to 60 T combined with pressures up to 4 GPa. We find a rich and complex phase diagram indicating a subtle competition between the electronic interactions. The main features are the disappearance of the field-induced SDW phase and a squeezing out of the HO phase under high pressure. We emphasize that many of the boundaries of the 3D phase diagram are controlled by the field- and pressure-dependences of a single parameter characterizing the electronic correlations.

Results

Zero-field phase diagram

Before tackling the question of the high-field properties of URu_2Si_2 under pressure, we recall in Figure 1(a) its zero-field (p,T) phase diagram (from data in Refs. [32],[44] and data shown in Figure S1, Supplementary Materials). The hidden-order and superconducting (SC) phases develop at ambient pressure below the temperatures T_0 = 17.5 K and T_{SC} = 1.5 K, respectively. Superconductivity is suppressed at the critical pressure p_c = 0.5 GPa, where a transition from the hidden order to long-range antiferromagnetism, delimited by the Néel temperature T_N, is observed. The upper temperature scale $T_\chi^{max} > T_N, T_0$, at which a broad maximum in the magnetic susceptibility χ for **H** || **c** is observed, indicates a crossover to a correlated paramagnetic (CPM) regime characterized by strong magnetic correlations. For $p > p_c$, T_0 slowly increases while T_N rises steeply under pressure, and a sequence AF → HO → CPM can be induced by increasing temperature. T_0 and T_N merge at the critical point (p^* = 1.3 GPa, T^* = 18 K), which separates the HO, AF, and CPM phases in the (p,T) phase diagram. For $p > p^*$, the hidden order has vanished and a direct sequence AF → CPM can be induced by increasing temperature. The fact that T_0, T_N, and T_χ^{max} all increase under pressure indicates that their associated energy scales are continuously enhanced.

Ambient-pressure high-field phase diagram

At ambient pressure a magnetic field leads to the destruction of the hidden order. The HO phase is replaced by a SDW phase preceding a polarized paramagnetic (PPM) regime, whose boundary can be defined through a crossover at the onset of a large magnetization $M >$ 1.4 μ_B/U (see Ref. [45]). The ambient pressure high-field phase diagram of URu_2Si_2 is shown in Figures 1(c) and 4(a). The SDW phase is delimited by sharp step-like increases at $\mu_0 H_1$ = 35 T and $\mu_0 H_3$ = 39 T (in rising fields) in the magnetization, which are the signatures of first-order metamagnetic transitions [45]. Inside the SDW phase, another first-order transition at $\mu_0 H_2$ = 37 T (in rising fields) is presumably related with a subtle change in the magnetic structure [38]. These boundaries are also visible in the resistivity ρ and its field-derivative $\partial\rho/\partial H$ [see Figures 2 and 3(a)]. At higher temperatures, a broad maximum in the resistivity is ascribed to the metamagnetic field H_m [45],[46]. The field H_m and the temperature T_χ^{max}, at

which the magnetic susceptibility also presents a broad maximum, delimit a CPM regime [38] similar to that of other heavy-fermion paramagnets (see review in Ref. [5]). The boundary of the CPM regime is not visible from $\partial M/\partial H$ versus H plots at temperatures $T < T_{\chi}^{max}$, where a broad maximum at $H_{\partial M/\partial H}^{max} > H_m$ delimits the high-field polarized regime. When the temperature is lowered, $H_{\partial M/\partial H}^{max}$ and H_m converge before the SDW phase develops [47]. Interestingly, the suppression of the 'high-temperature' correlated paramagnetism precedes that of the hidden order, indicating that the CPM regime is a precursor of the HO phase [45].

High-field phase boundaries under pressure

We describe here the low-temperature properties of URu_2Si_2 under combined pressure and magnetic field **H** || **c**. Figures 1(b-c) show the two-dimensional (2D) low-temperature (p,H) and the 3D (p,H,T) phase diagrams built here, from a large set of resistivity data presented in Figures 2 and 3(a), completed by data from Refs. [32],[40],[44],[48]. In particular, we detail how a magnetic field leads to the destabilization of the HO, SDW and AF ground states in favor of the PPM regime.

SDW phase boundaries: The upper boundary H_3 of the SDW phase is visible under pressures up to 1 GPa. However, no signature of H_1 can be found in our high-pressure data, possibly due to a stronger signal at the HO phase boundary H_0. No trace of H_1, H_2 or H_3 is seen for $p \geq 2$ GPa, indicating that pressure rapidly suppresses the field-induced SDW phase.

HO phase boundary: Under pressures $p = 0.6$ and 1 GPa, the field-destabilization of the HO phase precedes the SDW phase, and no sharp anomaly identifies H_0 which we have placed at a kink in $\partial\rho/\partial H$. For $2 \leq p < 2.9$ GPa, the transition at H_0 directly occurs between the HO and the PPM phases and the shape of the resistivity curve has changed. H_0 again is defined at a kink in $\partial\rho/\partial H$. As summarized in Figure 1(b), at low temperature H_0 increases almost linearly with p, reaching 47 T at $p = 2.9$ GPa.

AF phase boundary: At the highest pressures p = 3.6 and 3.9 GPa of this study, a sharp step-like anomaly in $\partial\rho/\partial H$ indicates a transition of different nature than at the lower pressures. Knowing that antiferromagnetism is stabilized under pressure, we assign this anomaly to the AF boundary. The AF critical field (defined at the mid of the step in $\partial\rho/\partial H$) equals $\mu_0 H_c$ = 48 T at p = 3.6 and 3.9 GPa. A difficulty comes from the non-observation in our resistivity data of the AF→HO transition at H_c in the pressure range $p_c \leq p < 3.6$ GPa. This transition at H_c was observed by neutron diffraction and dilatometry on stoichiometric URu_2Si_2 under pressure [33],[34],[48] and in the electrical resistivity of Fe-doped samples, for which a small orbital contribution, related to a high number of impurities, probably allowed the observation of an anomaly [49]. Interestingly, the extrapolation of the low-pressure H_c line (from [48]) ends at a critical point ($p^{**} \simeq 3.25$ GPa, $\mu_0 H^{**} \simeq 48$ T) where the low-pressure H_0 line transforms into the high-pressure H_c line. The low-temperature (p,H) phase diagram shown in Figure 1 (b) indicates that the field-induced HO phase has vanished beyond the critical point, i.e., under pressures $p > p^{**}$.

High-temperature effects

Figure 3 presents our resistivity data measured as function of magnetic field for a large collection of temperatures and pressures. Figure 4 shows isobar (H,T) phase diagrams constructed from our resistivity data at pressures p from 1 bar to 3.9 GPa (with complementary data from Refs. [40],[48]). The main features are described below. Both HO and AF critical fields H_0 and H_c decrease with increasing temperature and vanish at the temperatures T_0 and T_N, respectively. At all pressures, a broad maximum in $\rho(H)$ observed at high temperatures is identified as the signature of the pseudo-metamagnetic field H_m. H_m corresponds to a crossover between the low-field CPM regime and a high-field paramagnetic state. For $p \leq 1$ GPa, when the temperature is decreased H_m ends on top of the low-temperature SDW dome, and the strong anomalies in ρ at H_1, H_2, and H_3 mask that at H_m. The extrapolated low-temperature pseudo-metamagnetic field $\mu_0 H_m(T \rightarrow 0) = 36.5$ T lies within the SDW dome. For $2.1 \leq p \leq 2.9$ GPa, when T is reduced, H_m ends on top of the H_0

line, and the anomaly at H_0 hides that at H_m too. In this pressure range, we find an extrapolated value $\mu_0 H_m(T\rightarrow 0) \approx H_0$. For $p \geq 3.6$ GPa, H_m is clearly decoupled from H_c, but we lose again its trace at low temperatures, due to the high-field tail of the anomaly at H_c. Interestingly, $\mu_0 H_m(T\rightarrow 0)$ increases almost linearly under pressure, from 36.5 T at ambient pressure to 51.5 T at $p = 3.9$ GPa. We further find that the CPM regime, restricted to non-zero temperatures for $p < p^{**}$, extends down to the lowest temperatures in a narrow field window $H_c < H < H_m(T\rightarrow 0)$ for $p > p^{**}$ [see Figure 1(b)]. This decoupling of H_c and H_m indicates the nearby quantum antiferromagnetic instability, as already observed in heavy-fermion antiferromagnets [50],[51].

Orbital contribution to the resistivity

URu_2Si_2 being a compensated metal, its low-temperature high-field resistivity (in high-quality single crystals, as those investigated here) is controlled by the cyclotron motion of the carriers. For an isotropic Fermi surface, such orbital contribution to the resistivity is expected to diverge as H^2 in the high-field limit $\omega_c \tau \gg 1$, where ω_c is the cyclotron frequency and τ is the relaxation time. Deviations from this behavior are observed in URu_2Si_2 under a magnetic field **H** || **c**. At ambient pressure, the destruction of the hidden order at high temperature or in a high magnetic field is accompanied by a reduction of the carrier mobility and the orbital contribution to $\rho(H)$ vanishes [39],[41],[45],[52]. Fermi surface reconstructions inside the HO phase [53],[54],[55],[56],[57] make this orbital contribution continuously suppressed over a field-range of width $\simeq$ 5 T, leading to a broad and pronounced maximum of ρ at $H_\rho^{max,LT} < H_0$.

Figure 2 shows that the maximum in ρ is progressively weakened under pressures $p \leq 3.6$ GPa, and then almost suppressed at $p = 3.9$ GPa. At $p = 3.9$ GPa, the maximum in ρ is replaced by a broad plateau in ρ. This change of behavior is emphasized in a plot of $\partial\rho/\partial H$ versus H, where a minimum at $H_{\partial\rho/\partial H}^{min}$ for $p \leq 3.6$ GPa is replaced a continuous decrease of

$\partial\rho/\partial H$ at p = 3.9 GPa. The fact that the maximum at $H_\rho^{max,LT}$ survives at p = 3.6 GPa, where the field-induced hidden order is squeezed out, indicates that a strong orbital contribution, and possible associated Fermi surface reconstructions, are present in the AF phase. However, we cannot fully exclude an alternative picture where this maximum would be a signature of the HO phase, indicating then a possible coexistence of the AF and HO phases under combined fields and pressures.

Discussion

Importance of a single parameter δ

A striking feature of the 3D phase diagram of URu_2Si_2 is the high number of competing electronic states: two magnetically-ordered phases (antiferromagnetism and spin-density wave) and two magnetic regimes (correlated and polarized paramagnetisms), in addition to the HO and SC phases. Beyond this apparent complexity, we observe simple general trends: the fall of the main energy scales under magnetic field and their increase under pressure. As shown in Figure 5 (a), a plot of the magnetic-field-variation of T_χ^{max} and T_0 normalized by their zero-field values at ambient pressure shows that both quantities decrease and are almost proportional under magnetic field. Similarly, Figure 5 (b) presents a plot of the pressure variation of normalized values of T_χ^{max}, T_0, T_N (for $p > p^*$), H_0, and H_m, which indicates that they all increase and are quasi-proportional under pressure.

The quasi-proportionality between these different energy scales is confirmed by the plot of their ratios presented in Figure 6. Figure 6(a) shows that the ratio T_χ^{max} / T_0 is almost invariant under magnetic field and pressure. This plot indicates that the variations of the higher temperature scale T_χ^{max} drive those of T_0, and thus that the fall or stabilization of the CPM regime drives that of the HO phase. As shown in Figure 6(a), the ratio $R_{CPM} = T_\chi^{max}$ / ($\mu_0 H_m$) of the CPM regime boundaries is also invariant under pressure. Its value is close to the almost universal ratio $R_{CPM} = T_\chi^{max}$ / ($\mu_0 H_m$) $\simeq$ 1 K/T observed for a large number of heavy-fermion paramagnets and indicates a conventional behavior [5]. Similarly to R_{CPM}

introduced for the CPM regime, we define the characteristic ratio $R_{HO} = T_0 / (\mu_0 H_0)$ for the HO phase. Figure 6(c) shows that R_{HO} is constant under pressure, confirming that T_0 and H_0 increase in a proportional manner. For $p > p^*$, the proportionality of T_N with T_χ^{max}, H_0, and H_m is shown i) by the constant value of T_χ^{max} / T_N, which reaches a value $\simeq 3.5$ similar to that of T_χ^{max} / T_0 for $p < p^*$ [Figure 6(b)], and ii) by the constant values of $T_N / (\mu_0 H_0)$ and $T_N / (\mu_0 H_m)$ for $p > p^*$ and $p > p^{**}$, respectively, both reaching the same value $\simeq 0.5$ K/T than $R_{HO} = T_0 / (\mu_0 H_0)$ for $p < p^*$ [Figure 6(c)].

Their proportionality indicate that the pressure and magnetic field- variations of T_χ^{max}, T_0, T_N (for $p > p^*$), H_0, and H_m are controlled by those of a unique parameter, which we label δ. We discuss below what this parameter δ could be. In most of heavy-fermion paramagnets, the magnetic susceptibility χ (in a field applied along the easy magnetic axis) nearly saturates at temperatures smaller below T_χ^{max} and a Fermi liquid description is made within a first approximation. A naïve picture is to identify T_χ^{max} as the Fermi liquid temperature $T_F \propto 1/m^*$ of the heavy-fermion regime with an effective mass m^*. In such description, one parameter is controlling a large set of low temperature properties, as the heat capacity C_p and the magnetic susceptibility which verify $C_p/T \propto \chi \propto m^*$. From the relationship $R_{CPM} = T_\chi^{max} / (\mu_0 H_m) \simeq 1$ K/T evidenced for a large set of heavy-fermion paramagnets [5], it comes out that $m^* \propto 1 / T_\chi^{max} \propto 1 / H_m$. In addition, T_χ^{max} and H_m are almost proportional to the quasielastic line width Γ of intersite magnetic fluctuations in several heavy-fermion paramagnets, including URu_2Si_2 [5]. Thereafter, the effective mass m^* in URu_2Si_2 may be controlled by the magnetic fluctuations with wavevector $\mathbf{k}_1$ which develop in the CPM regime [9],[10]. Within this Fermi-liquid picture, the parameter δ driving the proportionality between the multiple phase boundaries in URu_2Si_2 could be the effective mass m^*. Of course, beyond this simple approach a more subtle description and several parameters are needed to describe all properties of the phase diagram.

All boundaries of the 3D phase diagram of URu_2Si_2 are not fully controlled by the parameter δ. A single energy scale is not sufficient to explain why the hidden order is replaced by antiferromagnetism under pressure, and the situation concerning the AF phase for $p < p^*$ is complex. As shown in Figure 6 (b), the strong variation of T_χ^{max} / T_N for $p < p^*$ shows that T_χ^{max} and T_N are not proportional. Figure 6(d) further indicates that the ratio $R_{AF} \simeq T_N / (\mu_0 H_c)$ characteristic of the AF boundaries varies strongly under pressure. It decreases with p for $p < p^*$, passes thought a minimum, and finally slightly increases for $p \gtrsim p^*$. This implies that several parameters are needed to relate the pressure-variations of T_N and H_c. Similar conclusion was found for a large number of heavy-fermion antiferromagnets [5],[50]. At ambient pressure, the temperature-dependent Grüneisen parameters reported in Ref. [58] also indicate that the parameter δ is not sufficient to describe all properties of URu_2Si_2.

However, a surprise here is to find that the HO boundaries T_0 and H_0, but also the AF Néel temperature T_N for $p > p^*$, are proportional to T_χ^{max} and H_m, and that their pressure- and magnetic-field- variations are driven by those of the same parameter δ. This, together with the fact that T_N for $p > p^*$ is a high-pressure prolongation of T_0 (see Figure 1), indicates that the antiferromagnetic and hidden orders have some common magnetic nature. Indeed, long-range order in the AF phase and gapped excitations in the HO phase have been observed with the same magnetic wavevector $\mathbf{k}_0$ [33],[34],[59]. An interplay between the magnetic and Fermi surface properties was also emphasized by the similar Fermi surfaces observed in the two states, for which a simple tetragonal symmetry has been proposed [19],[60].

New constraints for a microscopic description

Two models proposed a description of the field-induced reentrance of the hidden order in URu_2Si_2 under pressure: i) a phenomenological Landau-Ginzburg theory based on LDA+DMFT calculation, where the hidden order was identified as a hexadecapole with periodicity $\mathbf{k}_0$, [27], and a spin-liquid model based on correlations with wavevector $\mathbf{k}_0$ [28]. A question is whether these models, as well as other propositions for the HO phase [26],[29],[30], could be adjusted to describe the full 3D phase diagram of URu_2Si_2. Although

the purpose of discriminating the different existing theories is beyond the scope of this paper, the phase diagram reported here imposes new constraints. We detail below these constraints.

The main results of our work are the observed suppressions of the field-induced SDW state under moderate pressure and of the field-induced HO state under high pressure. A critical point at ($p^{**} \simeq 3.25$ GPa, $\mu_0 H^{**} \simeq 48$ T) can be defined at the crossing of the H_0 line observed for $p < p^{**}$ and the decoupled H_c and H_m lines observed for $p > p^{**}$. This point (p^{**},H^{**}) lies just on the linear extrapolation of the low pressure H_c transition and separates four states: the AF and HO phases and the CPM and PPM regimes. Recent studies on Fe-doped URu_2Si_2 reported a similar phase diagram, with a strengthening of antiferromagnetism with increased doping and a field-induced reentrance of the hidden order [37],[49],[61]. A theory aiming to describe the hidden order in URu_2Si_2 would need to reproduce the various features in its 3D phase diagram, i.e., the way the HO phase competes with other ordered (AF, SDW) phases or paramagnetic (CPM, PPM) regimes.

Although URu_2Si_2 has a rich and complex 3D electronic phase diagram, we have seen that many of its boundaries (T_χ^{max}, T_0, H_m, H_0, and T_N for $p > p^*$) vary proportionally and are controlled by the pressure- or magnetic-field variation of a unique parameter δ. We have discussed that, within a Fermi liquid description of the CPM regime, the effective mass m^*, possibly controlled by magnetic fluctuations with wavevector $\mathbf{k}_1$ [9],[10], could be a realization of δ. However, the magnetic fluctuations are strongly modified in the HO phase, and a single parameter is not sufficient to describe the gapped excitations reported at the two wavevectors $\mathbf{k}_0$ and $\mathbf{k}_1$ [10],[40],[59]. The relative roles played by the correlations with the wavevector $\mathbf{k}_1$ in the CPM regime, as well as the sharp and inelastic fluctuations with the wavevectors $\mathbf{k}_0$ and $\mathbf{k}_1$ in the HO phase, might be clarified. How do they contribute to the mass enhancement? How these correlations evolve and drive the phase boundaries under pressure and magnetic field?

For such purpose, a description of the Fermi surface and its evolution under combined pressures and magnetic fields is important. From Shubnikov-de-Haas experiments, a cascade of Fermi surface reconstructions under magnetic field was reported

[39],[41],[52],[53],[54],[55], while no Fermi-surface reconstruction was observed under pressure at low field [19]. Fermi-surface-driven changes of RKKY magnetic exchange interactions $J_{ex}(\mathbf{k})$ may lead to the appearance of long-range magnetic order, either antiferromagnetism with wavevector $\mathbf{k}_0$ or spin-density wave with wavevector $\mathbf{k}_1$, under pressure and magnetic field, respectively. Within this picture, pressure-enhanced exchange $J_{ex}(\mathbf{k}_0)$ would result in antiferromagnetic order with wavevector $\mathbf{k}_0$, while magnetic-field-enhanced exchange $J_{ex}(\mathbf{k}_1)$ would lead to a spin-density wave with wavevector $\mathbf{k}_1$. These magnetic orders could be accompanied by Fermi surface nestings with their respective wavevectors $\mathbf{k}_0$ and $\mathbf{k}_1$. The gapped magnetic excitations with the wavevectors $\mathbf{k}_0$ and $\mathbf{k}_1$ reported at ambient pressure and zero-field [9],[10] could be related to inelastic nestings with the same wavevectors of the electronic band. To our knowledge, the origin of the RKKY interactions $J_{ex}(\mathbf{k}_0)$ and $J_{ex}(\mathbf{k}_1)$ was not modeled so far. Understanding how these exchange parameters and the related magnetic excitations evolve under pressure and magnetic field would allow identifying the parameter δ and describing the 3D phase diagram reported here. This could constitute a decisive step in the search for a consensus about the nature of the hidden order.

Methods

URu_2Si_2 single crystals measured here were grown by the Czochralski technique in a tetra-arc furnace. Their electrical resistivity (contacts along **a**) of samples #A and #B has been measured under magnetic fields up to 58 T applied along **c** combined with pressures up to 3.9 GPa and temperatures down to 1.5 K. The residual resistivity ratio RRR = $\rho_{x,x}$(300 K)/ $\rho_{x,x}$(2 K), defined at zero field by the ratio of the resistivities at 300 K and 2 K, i.e., just above the superconducting temperature, was equal to $\simeq$ 110 for both samples #A and #B, indicating their high quality. Resistivity was measured using the four-contact technique, with an excitation current of 10 mA at a frequency of $\simeq$ 50-70 kHz. A Bridgman-type pressure cell specially designed for the pulsed fields has been used. To avoid significant heating by eddy currents, ceramic anvils and a pyrophilit gasket were used in the cell, whose body is made of MP35N. The data presented here correspond to the rise of the field pulses, where maximal

heating is estimated, for 58-T pulses, to be less that 0.1 K at temperatures $T \leq 4.2$ K, close to 1-1.5 K at temperatures from 5 K to 20 K, and negligible at higher temperatures. For lower-field pulses, the heating effects are reduced. We note that, in addition to heating effects by eddy-current generated in the body of the cell, small deviations from an isothermal limit due to magnetocaloric cooling effect cannot be excluded. Magnetocaloric effects can be observed in large samples of several-mm dimensions under pulsed magnetic fields, for which an adiabatic limit allows the sample temperature to change. Here, thin samples of thickness of typically 50 µm were measured and long-duration pulse-fields (rise of 55 ms, total duration > 300 ms) were used, which constitute favorable conditions for a quasi-isothermal limit. Pressure was estimated by measuring the resistance of a lead gage simultaneously to the resistance of the URu_2Si_2 sample. More information about the pressure cell setup can be found in two technical papers [42],[43]. Complementary resistivity measurements have been made on a third sample (sample #C, RRR = 60) under pressures up to 4 GPa in steady fields up to 14 T using a Physical Properties Measurements System from Quantum Design.

Acknowledgments

We acknowledge Jacques Flouquet for discussions and critical reading of the paper, and Sébastien Burdin for discussions. The work at the LNCMI was supported by the 'Programme Investissements d' Avenir' under the project NEXTREME / NEXT (program ANR-11-IDEX-0002-02, reference ANR-10-LABX-0037-NEXT). We acknowledge the Propulse Program, the Program for Advancing Strategic International Networks to Accelerate the Circulation of Talented Researchers from JSPS (R2705), and the KAKENHI program (JP15H05882, JP15H05884, JP15K21732, JP19H00646,JP15H05745).

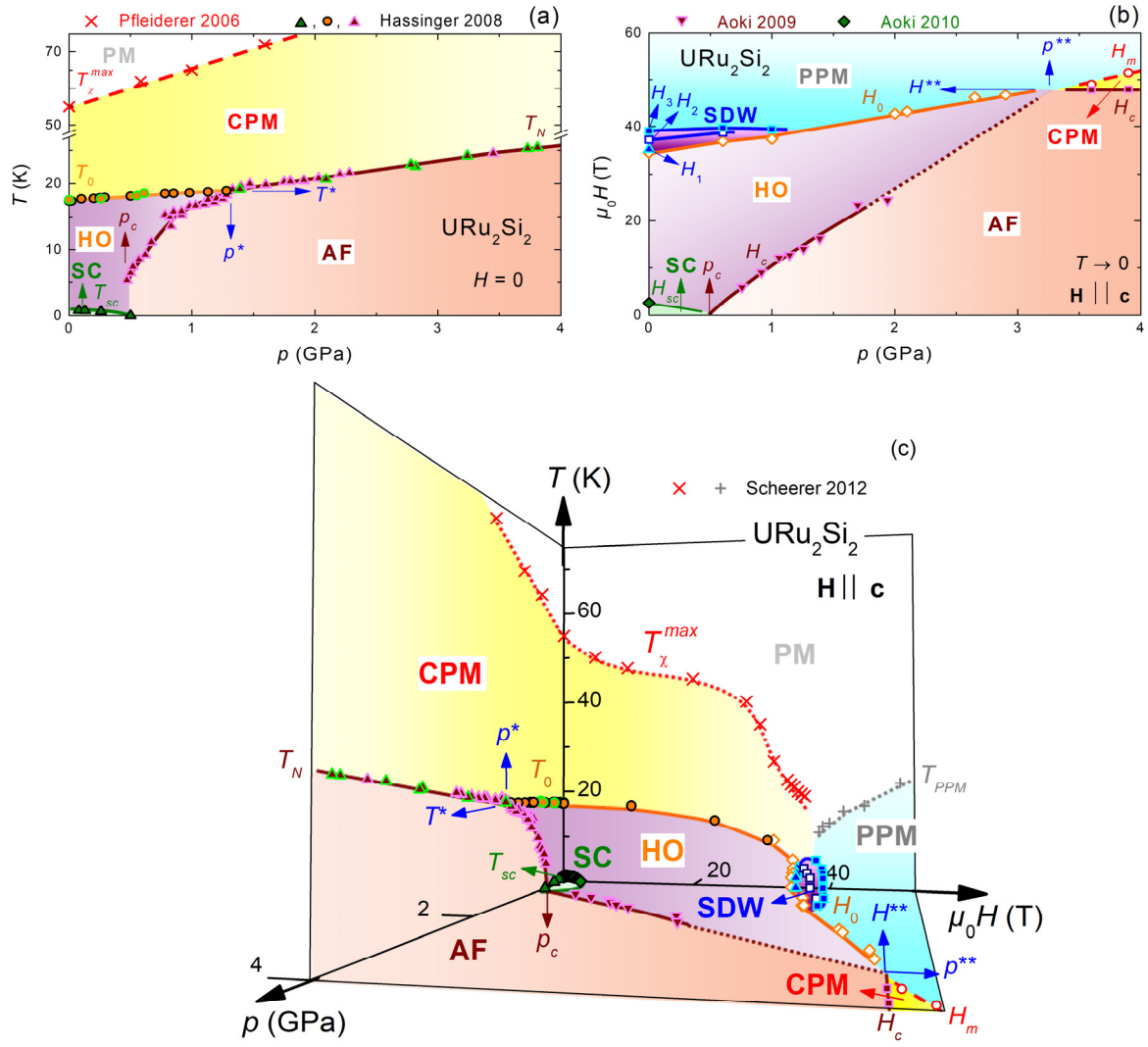

Figure 1. Electronic phase diagram of URu_2Si_2 under pressure and magnetic field H || c. (a) Temperature – pressure phase diagram at zero field, (b) magnetic field – pressure phase diagram in the limit $T \rightarrow 0$, (c) temperature - pressure - magnetic field phase diagram. PM, CPM, and PPM are the high-temperature, the low-temperature correlated, and the high-field polarized paramagnetic regimes, respectively, HO and SC the hidden-order and superconducting phases, respectively, AF the antiferromagnetic state, and SDW the spin-density wave state. In addition to data from this work, data from Refs. [32],[40],[44],[45],[48] (data points from these works and their references are indicated in the Figure) were used to construct these phase diagrams.

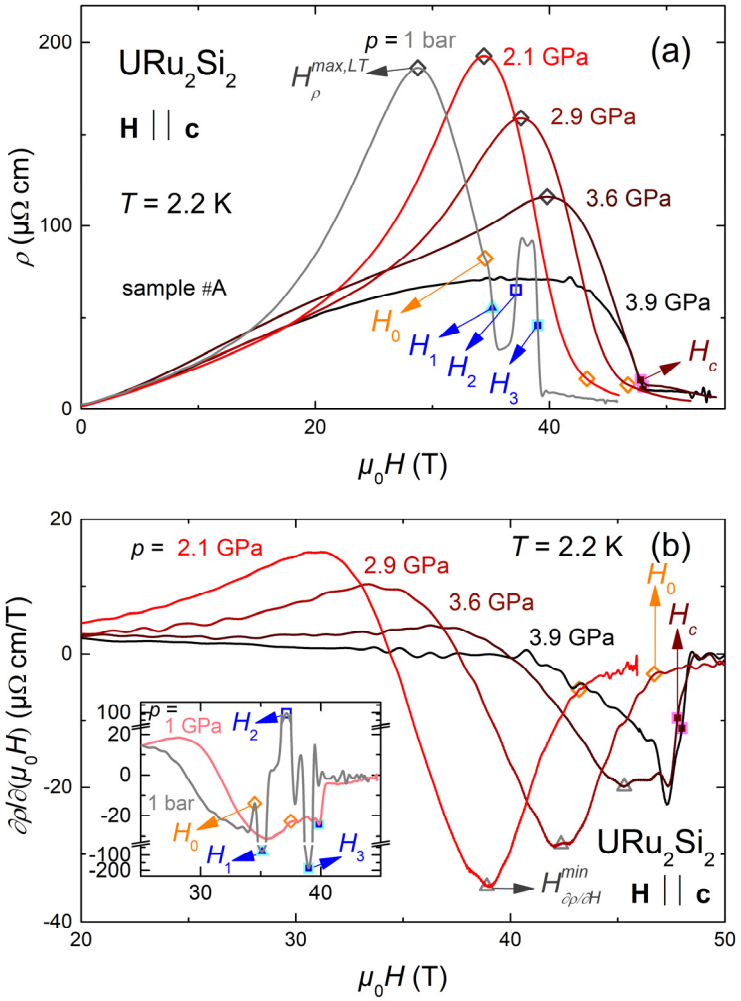

Figure 2. Low-temperature resistivity ρ and its derivative $\partial\rho/\partial H$ of URu_2Si_2 versus magnetic field H || c at different pressures. (a) ρ versus H and (b) $\partial\rho/\partial H$ versus H at different pressures p from 1 bar to 3.9 GPa, at $T = 2.2$ K.

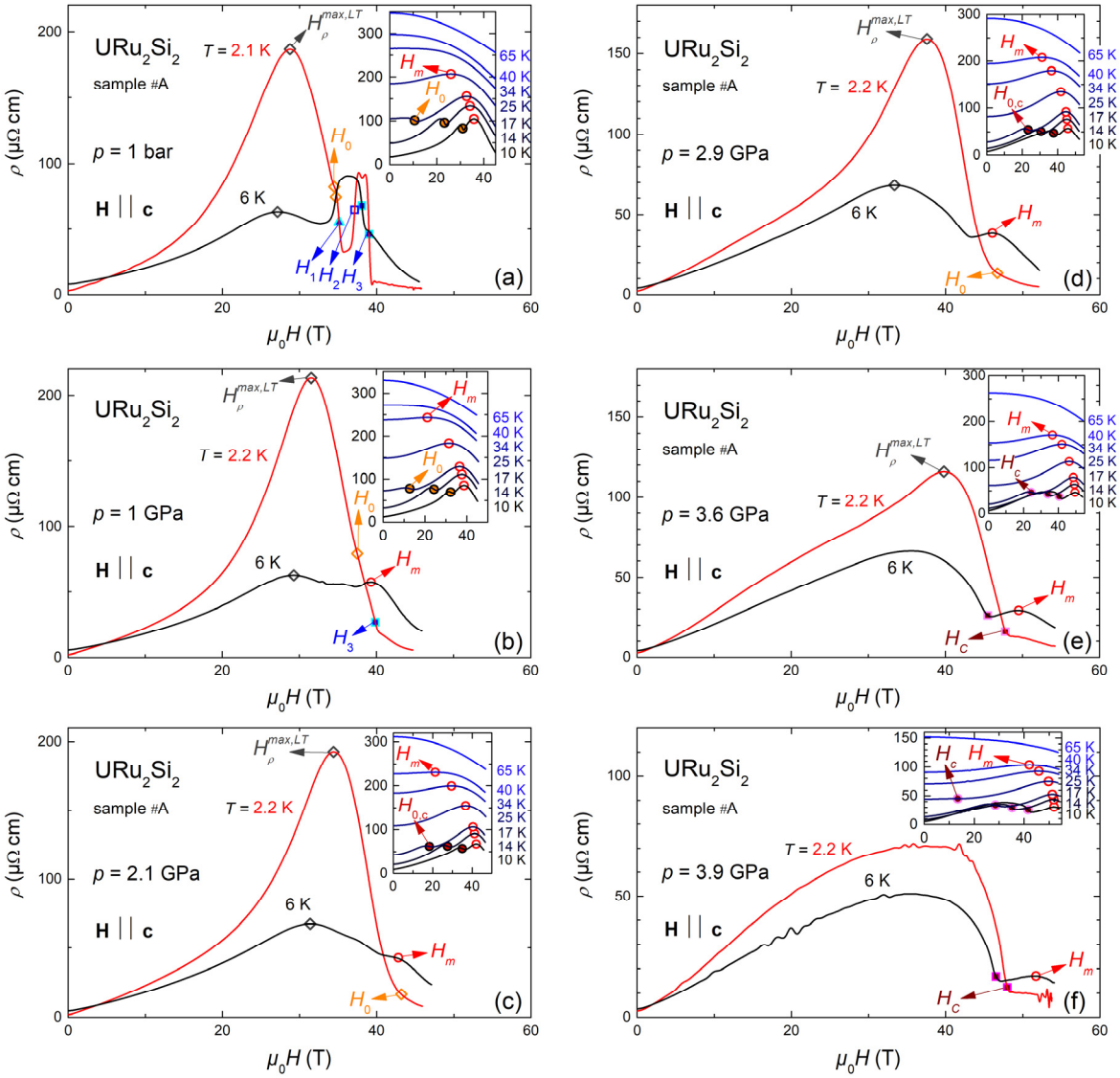

Figure 3. **Resistivity ρ of URu_2Si_2 versus magnetic field H || c at different temperatures and pressures.** ρ versus H at temperatures T from 2.2 to 65 K, at the pressures p = (a) 1 bar, (b) 1GPa, (c) 2.1 GPa, (d) 2.9 GPa, (e) 3.6 GPa, and (f) 3.9 GPa. The insets present high-temperatures data while the main graphs present low-temperature data.

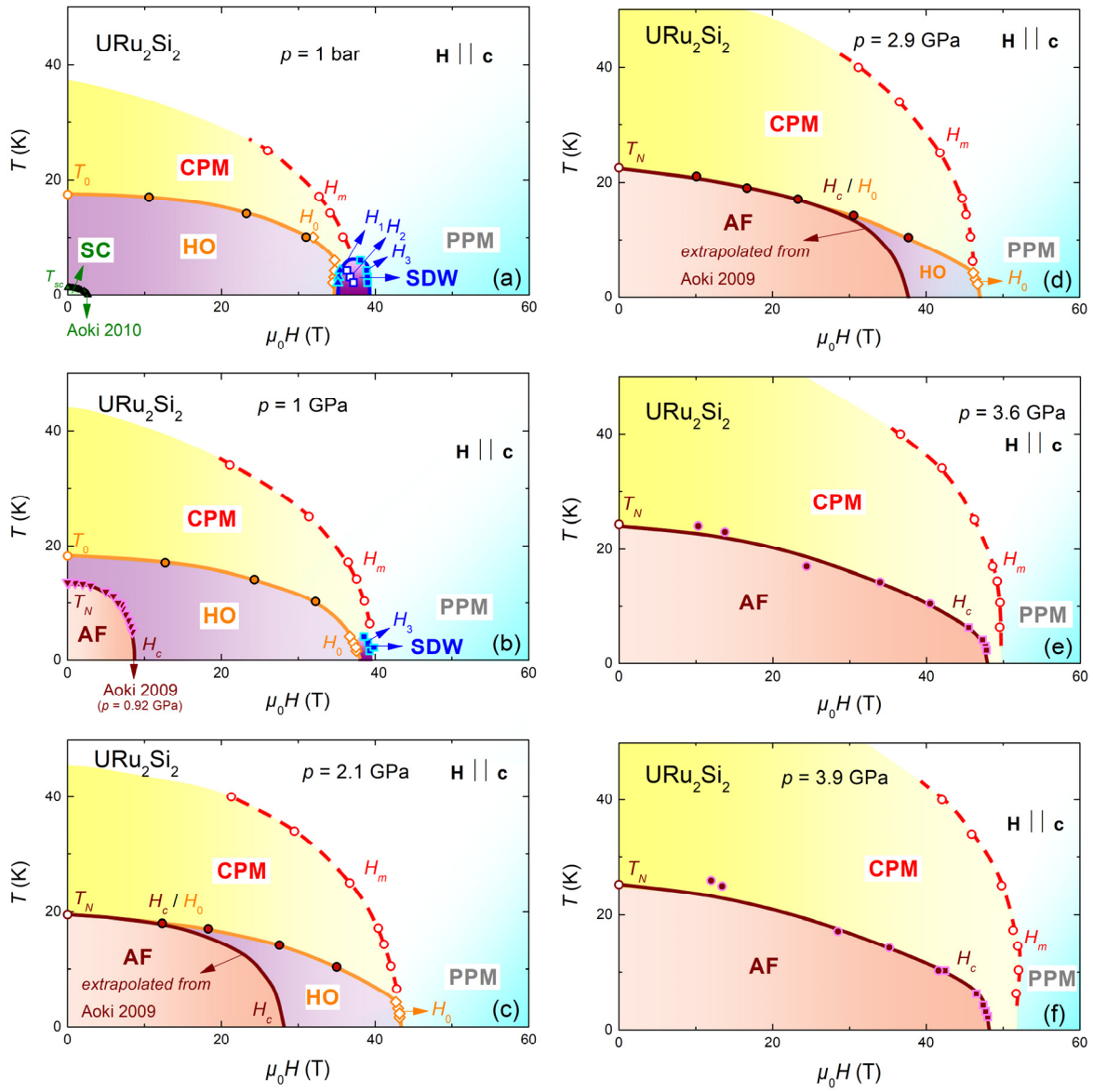

Figure 4. **Magnetic field-temperature phase diagrams of URu_2Si_2 under pressure and magnetic field H || c.** Magnetic phase diagrams obtained at the pressures p = (a) 1 bar, (b) 1GPa, (c) 2.1 GPa, (d) 2.9 GPa, (e) 3.6 GPa, and (f) 3.9 GPa.. PM, CPM, and PPM are the high-temperature, the low-temperature correlated, and the high-field polarized paramagnetic regimes, respectively, HO and SC the hidden-order and superconducting phases, respectively, AF the antiferromagnetic state, and SDW the spin-density wave state. In addition to data from this work, data from Refs. [32],[40],[44],[48] were used to construct these phase diagrams.

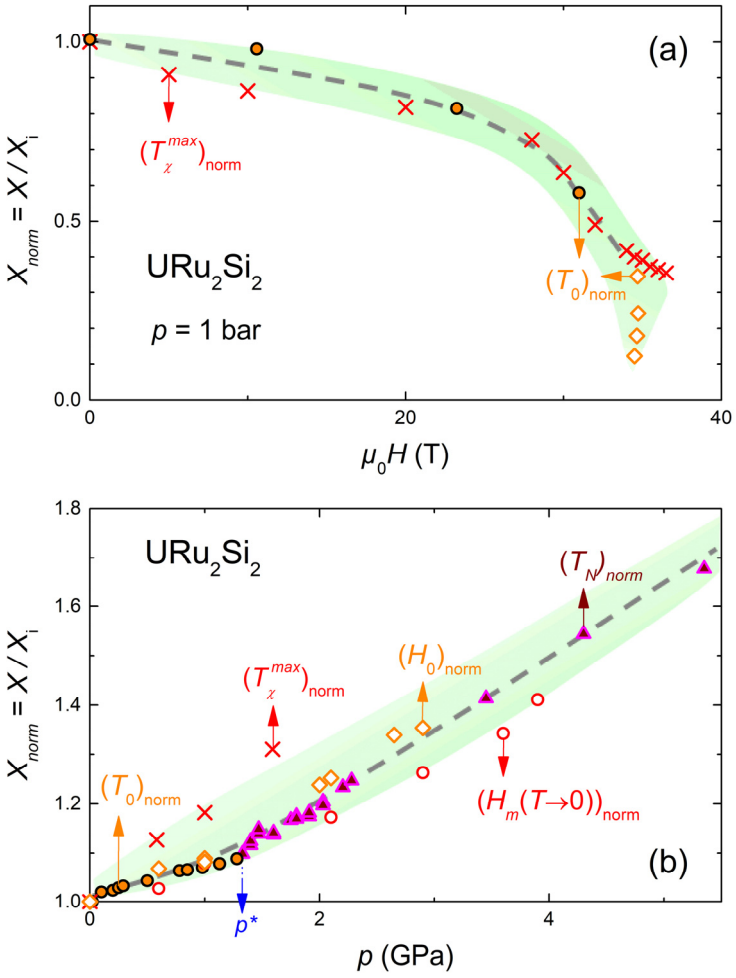

Figure 5. Field- and pressure-variations of normalized characteristic temperatures and magnetic fields. (a) Plot of normalized values of T_{χ}^{max} and T_0 versus H, (b) plot of normalized values of T_{χ}^{max} , T_0, T_N, H_0, and H_m versus p.

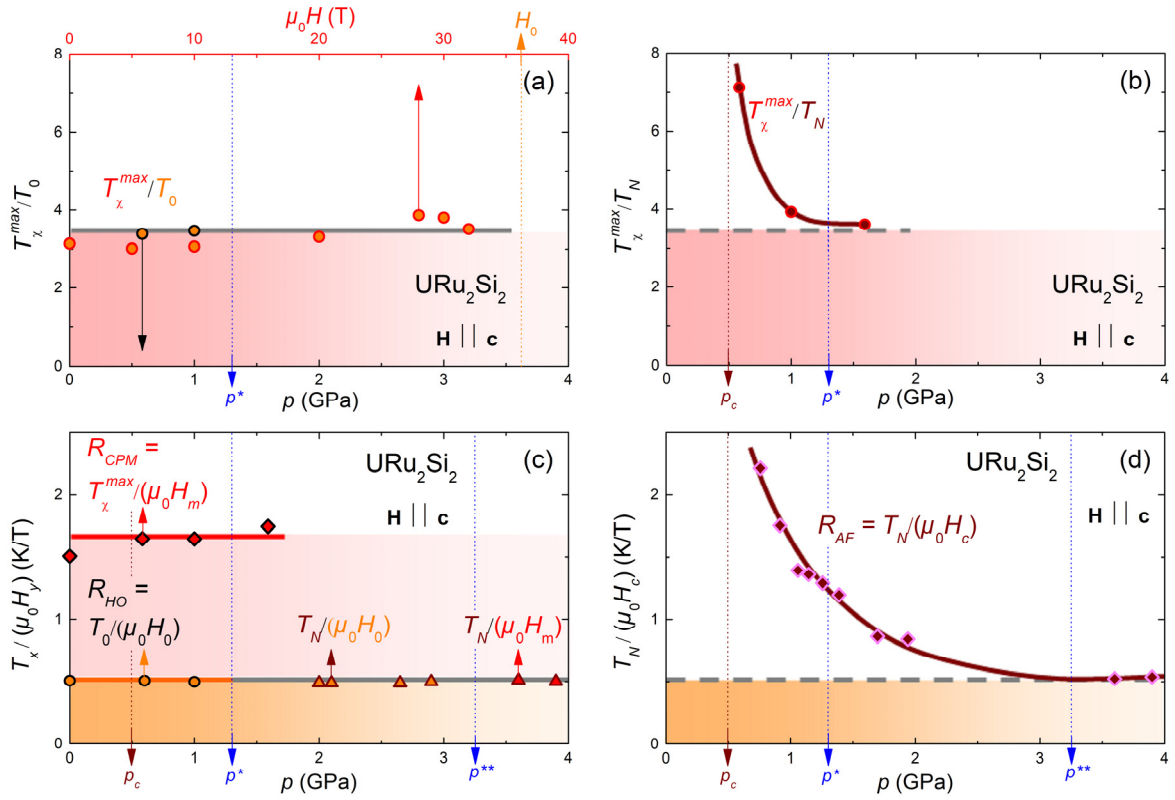

Figure 6. Field- and pressure-variations of characteristic temperature and magnetic-field ratios. Plots of (a) T_χ^{max} / T_0 versus H and p, (b) T_χ^{max} / T_N versus p, (c) $R_{CPM} = T_\chi^{max} / (\mu_0 H_m)$, $R_{HO} = T_0 / (\mu_0 H_0)$, $T_N / (\mu_0 H_0)$, and $T_N / (\mu_0 H_m)$ versus p, *(d)* $R_{AF} \simeq T_N / (\mu_0 H_c)$ versus p. T_χ^{max} is the temperature at which the magnetic susceptibility is maximal. H_m is the metamagnetic field. T_0 and H_0 are the boundaries of the hidden-order phase. T_N and H_c are the boundaries of the antiferromagnetic phase.

References

[1] Armitage, N.P., Fournier, P., & Greene, R.L., Progress and perspectives on electron-doped cuprates. *Rev. Mod. Phys.* **82**, 2421 (2010).

[2] Johnston, D.C., The puzzle of high temperature superconductivity in layered iron pnictides and chalcogenides. *Adv. Phys.* **59**, 803 (2010).

[3] Flouquet, J., On the heavy-fermion road. *Prog. Low Temp. Phys*. **15**, 139-281 (2005).

[4] von Löhneysen, H., Rosch, A., Vojta, M. & Wölfle, P. Fermi-liquid instabilities at magnetic quantum phase transitions. *Rev. Mod. Phys.* **79**, 1015-1075 (2007).

[5] Aoki, D., Knafo, W., & Sheikin, I. Heavy fermions in a high magnetic field. *C. R. Physique* **14**, 53–77 (2013).

[6] Pfleiderer, C., Superconducting phases of f -electron compounds. *Rev. Mod. Phys.* **81**, 1551 (2009)

[7] Mydosh, J. A., & Oppeneer, P. M., Colloquium: Hidden order, superconductivity, and magnetism: The unsolved case of URu_2Si_2. *Rev. Mod. Phys.* **83**, 1301 (2011).

[8] Palstra, T.T.M., Menovsky, A.A., van den Berg, J., Dirkmaat, A. J., Kes, P.H., Nieuwenhuys, G.J., & Mydosh, J.A. Superconducting and Magnetic Transitions in the Heavy-Fermion System URu_2Si_2. *Phys. Rev. Lett.* **55**, 2727 (1985).

[9] Broholm, C., Lin, H., Matthews, P. T., Mason, T. E., Buyers, W. J. L., Collins, M. F., Menovsky, A. A., Mydosh, J. A., & Kjems, J. K., Magnetic excitations in the heavy-fermion superconductor URu_2Si_2. *Phys. Rev. B* **43**, 12809 (1991).

[10] Bourdarot, F., Raymond, S. Regnault, L.-P., Neutron scattering studies on URu_2Si_2. *Philos. Mag.* **94**, 3702 (2014).

[11] LeR. Dawson, A., Datars, W.R., Garrett, J.D., & Razavi, F.S. Electrical transport in URu_2Si_2. *J. Phys. Condens. Matter* **1**, 6817 (1989).

[12] Bel, R. , Jin, H., Behnia, K., Flouquet, J., & Lejay, P. Thermoelectricity of URu_2Si_2: Giant Nernst effect in the hidden-order state. *Phys. Rev. B* **70**, 220501 (2004).

[13] Kasahara, Y., Iwasawa, T., Shishido, H., Shibauchi, T., Behnia, K., Haga, Y., Matsuda, T.D., Onuki, Y., Sigrist, M., & Matsuda, Y. Exotic superconducting properties in the electron-hole-compensated heavy-fermion "semimetal" URu_2Si_2. *Phys. Rev. Lett*. **99**, 116402 (2007).

[14] Santander-Syro, A. F., Klein, M., Boariu, F. L., Nuber, A., Lejay, P., & Reinert, F. Fermi-surface instability at the 'hidden-order' transition of URu_2Si_2. *Nature Phys*. **5**, 637–641 (2009).

[15] Schmidt, A.R., Hamidian, M.H., Wahl, P., Meier, F., Balatsky, A.V., Garrett, J.D., Williams, T.J., Luke, G.M., & Davis, J. C. Imaging the Fano lattice to 'hidden order' transition in URu_2Si_2. *Nature* **465**, 570–576 (2010).

[16] Aynajian, P., da Silva Neto, A.H., Parker, C.V., Huang, Y., Pasupathy, A., Mydosh, J., & Yazdani, A. Visualizing the formation of the Kondo lattice and the hidden order in URu_2Si_2. *Proc. Natl. Acad. Sci. USA* **110**, 10383-10388 (2010).

[17] Broholm, C., Kjems, J. K., Buyers, W. J. L., Matthews, P., Palstra, T. T. M., Menovsky, A. A., & Mydosh, J. A. Magnetic excitations and ordering in the heavy-electron superconductor URu_2Si_2. *Phys. Rev. Lett.* **58**, 1467 (1987).

[18] Niklowitz, P. G., Pfleiderer, C., Keller, T., Vojta, M., Huang, Y.-K., & Mydosh, J. A. Parasitic Small-Moment Antiferromagnetism and Nonlinear Coupling of Hidden Order and Antiferromagnetism in URu_2Si_2 Observed by Larmor Diffraction. *Phys. Rev. Lett.* **104**, 106406 (2010).

[19] Hassinger, H., Knebel, G., Matsuda, T.D., Aoki, D., Taufour, V., & Flouquet, J. Similarity of the Fermi Surface in the Hidden Order State and in the Antiferromagnetic State of URu_2Si_2. *Phys. Rev. Lett.* **105**, 216409 (2010).

[20] Okazaki, R., Shibauchi, T., Shi, H. J., Haga, Y., Matsuda, T. D., Yamamoto, E., Onuki, Y., Ikeda, H., & Matsuda, Y. Rotational Symmetry Breaking in the Hidden-Order Phase of URu_2Si_2. *Science* **331**, 439 (2011).

[21] Tonegawa, S., Kasahara, S., Fukuda, T., Sugimoto, K., Yasuda, N., Tsuruhara, Y., Watanabe, D., Mizukami, Y., Haga, Y., Matsuda, T. D., Yamamoto, E., Onuki, Y., Ikeda, H., Matsuda, & Y., Shibauchi, T. Direct observation of lattice symmetry breaking at the hidden-order transition in URu_2Si_2. *Nature Commun.* **5**, 4188 (2013).

[22] Choi, J., Ivashko, O., Dennler, N., Aoki, D., von Arx, K., Gerber, S., Gutowski, O., Fischer, M.H., Strempfer, J., v. Zimmermann, M., & Chang, J. Pressure-induced rotational symmetry breaking in URu_2Si_2. *Phys. Rev. B* **98**, 24113(R) (2018).

[23] Tabata, C., Inami, T., Michimura, S., Yokoyama, Hidaka, M.H., Yanagisawa, T., & Amitsuka, H. X-Ray Backscattering Study of Crystal Lattice Distortion in Hidden Order of URu_2Si_2. *Philos. Mag.* **94**, 3691 (2014).

[24] Kambe, S., Tokunaga, Y., Sakai, H., Hattori, T., Higa, N., Matsuda, T.D., Haga, Y., Walstedt, R.E., & Harima, H. Odd-parity electronic multipolar ordering in URu_2Si_2: Conclusions from Si and Ru NMR measurements. *Phys. Rev. B* **97**, 235142 (2018).

[25] Wang, L., He, M., Hardy, F., D. Aoki, Willa, K., Flouquet, J., & Meingast, C. Electronic nematicity in URu_2Si_2 revisited, to be published.

[26] Fujimoto, S. Spin Nematic State as a Candidate of the Hidden Order Phase of URu_2Si_2. *Phys. Rev. Lett.* **106**, 196407 (2011)

[27] Haule, K., & Kotliar, G. Complex Landau-Ginzburg theory of the hidden order in URu_2Si_2. *Europhys. Lett.* **89**, 57006 (2010).

[28] Thomas, C., Burdin, S., Pépin, C., & Ferraz, A. Three-dimensional modulated spin liquid model applied to URu_2Si_2. *Phys. Rev. B* **87**, 014422 (2013).

[29] Chandra, P., Coleman, P., & Flint, R. *Nature* **493**, 621, (2013).

[30] Ikeda, H., Suzuki, M.-T., Arita, R., Takimoto, T., Shibauchi, T. & Matsuda, Y. Emergent rank-5 nematic order in URu_2Si_2, *Nature Phys.* **8**, 528–533 (2012).

[31] Knafo, W., Raymond, S., Lejay, P., & Flouquet, J. Antiferromagnetic criticality at a heavy-fermion quantum phase transition. *Nature Phys*. **5**, 753–757 (2009).

[32] Hassinger, E., Knebel, G., Izawa, K., Lejay, P., Salce, B., and Flouquet, J. Temperature-pressure phase diagram of URu_2Si_2 from resistivity measurements and ac calorimetry: Hidden order and Fermi-surface nesting. *Phys. Rev. B* **77**, 115117 (2008).

[33] Bourdarot, F., Bombardi, A., Burlet, P., Enderle, M., Flouquet, J., Lejay, P., Kernavanois, N., Mineev, V.P., Paolasini, L., Zhitomirsky, M.E.,& Fåk, B. Hidden order in URu_2Si_2. *Physica B* **359-361**, 986-993 (2005).

[34] Amitsuka, H., Matsuda, K., Kawasaki, I., Tenya, K., Yokoyama, M., Sekine, C., Tateiwa, N., Kobayashi, T.C., Kawarazaki, S., &Yoshizawa, H. Pressure–temperature phase diagram of the heavy-electron superconductor URu_2Si_2. *J. Magn. Magn. Mater.* **310**, 214-220 (2007).

[35] Bourdarot, F., Martin, N., Raymond, S., Regnault, L.-P., Aoki, D., Taufour, V., & Flouquet, J. Magnetic properties of URu_2Si_2 under uniaxial stress by neutron scattering. *Phys. Rev. B* **84**, 184430 (2011).

[36] Yokoyama, M., Amitsuka, H., Itoh, S., Kawasaki, I., Tenya, K., & Yoshizawa, H. Neutron Scattering Study on Competition between Hidden Order and Antiferromagnetism in $U(Ru_{1-x}Rh_x)_2Si_2$ ($x \leq 0.05$). *J. Phys. Soc. Jpn.* **73**, 545-548 (2004).

[37] Das, P., Kanchanavatee, N., Helton, J.S., Huang, K., Baumbach, R.E., Bauer, E.D., White, B.D., Burnett, V.W., Maple, M.B., Lynn, J.W., & Janoschek, M. Chemical pressure tuning of URu_2Si_2 via isoelectronic substitution of Ru with Fe. *Phys. Rev. B* **91**, 085122 (2015).

[38] Knafo, W., Duc, F., Bourdarot, F., Kuwahara, K., Nojiri, H., Aoki, D., Billette, J., Frings, P., Tonon, X., Lelièvre-Berna, E., Flouquet, J., & Regnault, L.-P. Field-induced spin-density wave beyond hidden order in URu_2Si_2. *Nature Commun*. **7**, 13075 (2016).

[39] Knafo, W., Aoki, D., Scheerer, G.W., Duc, F., Bourdarot, F., Kuwahara, K., Nojiri, H., Regnault, L.-P. , & Flouquet, J. URu_2Si_2 under intense magnetic fields: from hidden order to spin-density wave. *Physica B* **536**, 457 (2018).

[40] Aoki, D., Bourdarot, F., Hassinger, E., Knebel, G., Miyake, A., Raymond, S., Taufour, V., & Flouquet, J. Field Reentrance of the Hidden Order State of URu_2Si_2 under Pressure. *J. Phys. Soc. Jpn.* **78**, 053701 (2009).

[41] Jo, Y.J., Balicas, L., Capan, C., Behnia, K., Lejay, P., Flouquet, J., Mydosh, J.A., & Schlottmann, P. Field-Induced Fermi Surface Reconstruction and Adiabatic Continuity between Antiferromagnetism and the Hidden-Order State in URu_2Si_2. *Phys. Rev. Lett.* **98**, 166404 (2007).

[42] Braithwaite, D., Knafo, W., Settai, R., Aoki, D., Kurahashi, S., & Flouquet, J. Pressure cell for transport measurements under high pressure and low temperature in pulsed magnetic fields, *Rev. Sci. Instrum.* **87**, 023907 (2016).

[43] Settai, R., Knafo, W., Braithwaite, D., Kurahashi, S., Aoki, D., & Flouquet, J. Development of Bridgman-Type Pressure Cell for Pulsed High Magnetic Field, *Review of High Pressure Science and Technology / Koatsuryoku No Kagaku To Gijutsu* **25**, 325 (2015).

[44] Pfleiderer, C., Mydosh, J. A., & Vojta, M. Pressure dependence of the magnetization of URu_2Si_2. *Phys. Rev. B* **74**, 104412 (2006).

[45] Scheerer, G. W., Knafo, W., Aoki, D., Ballon, G., Mari, A., Vignolles, D., & Flouquet, J. Interplay of magnetism, Fermi surface reconstructions, and hidden order in the heavy-fermion material URu_2Si_2. *Phys. Rev. B* **77**, 115117 (2012).

[46] Kim, K.H., Harrison, N., Jaime, M., Boebinger, G.S., & Mydosh, J.A. Magnetic Field-Induced Quantum Critical Point and Competing Order Parameters in URu_2Si_2. *Phys. Rev. Lett.* **91**, 256401 (2003).

[47] Sugiyama, K., Nakashima, M., Ohkuni, H., Kindo, K., Haga, Y., Honma, T., Yamamoto, E. , Ōnuki, Y. Metamagnetic Transition in a Heavy Fermion Superconductor URu_2Si_2. *J. Phys. Soc. Jpn.* **68**, 3394-3401 (1999).

[48] Aoki, D., Bourdarot, F., Hassinger, E., Knebel, G., Miyake, A., Raymond, S., Taufour, V., & Flouquet, J. Field re-entrant hidden-order phase under pressure in URu_2Si_2. *J. Phys.: Condens. Matter* **22**, 164205 (2010).

[49] Ran, S., Jeon, I., Pouse, N., Breindel, A.J., Kanchanavatee, N., Huang, K., Gallagher, A., Chen, K.-W., Graf, D., Baumbach, R.E., Singleton, J., & Maple, M.B. Phase diagram of $URu_{2-x}Fe_xSi_2$ in high magnetic fields. *Proc Natl Acad Sci U S A* **114**, 9826-9831 (2017).

[50] Knafo, W., Settai, R., Braithwaite, D., Kurahashi, S., Aoki, D., & Flouquet, J. Three-dimensional critical phase diagram of the Ising antiferromagnet $CeRh_2Si_2$ under intense magnetic field and pressure, *Phys. Rev. B* **95**, 014411 (2017).

[51] Aoki, D., Paulsen, C., Kotegawa, H., Hardy, F., Meingast, C., Haen, P., Boukahil, M., Knafo, W., Ressouche, E., Raymond, S., & Flouquet, J. Decoupling between field-instabilities of antiferromagnetism and pseudo-metamagnetism in Rh-doped $CeRu_2Si_2$ Kondo lattice. *J. Phys. Soc. Jpn.* **81**, 034711 (2012).

[52] Scheerer, G. W., Knafo, W., Aoki, D., Nardone, M., Zitouni, A., Béard, J., Billette, J., Barata, J., Jaudet, C., Suleiman, M., Frings, P., Drigo, L., Audouard, A., Matsuda, T. D., Pourret, A., Knebel, G., & Flouquet, J. Fermi surface in the hidden-order state of URu_2Si_2 under intense pulsed magnetic fields up to 81 T. *Phys. Rev. B* **89**, 165107 (2014).

[53] Shishido, H., Hashimoto, K., Shibauchi, T., Sasaki, T., Oizumi, H., Kobayashi, N., Takamasu, T., Takehana, K., Imanaka, Y., Matsuda, T.D., Haga, Y., Onuki, Y., & Matsuda, Y. Possible Phase Transition Deep Inside the Hidden Order Phase of Ultraclean URu_2Si_2. *Phys. Rev. Lett.* **102**, 156403 (2009).

[54] Altarawneh, M.M., Harrison, N., Sebastian, S.E., Balicas, L., Tobash, P.H., Thompson, J.D., Ronning, F., & Bauer, E.D. Sequential Spin Polarization of the Fermi Surface Pockets in URu_2Si_2 and Its Implications for the Hidden Order. *Phys. Rev. Lett.* **106**, 146403 (2011).

[55] Harrison, N., Moll, P.J.W., Sebastian, S.E., Balicas, L., Altarawneh, M.M., Zhu, J.-X., Tobash, P.H., Ronning, F., Bauer, E.D., & Batlogg, B. Magnetic field-tuned localization of the 5f-electrons in URu_2Si_2. *Phys. Rev. B* **88**, 241108(R) (2013).

[56] Aoki, D., Knebel, G., Sheikin, I., Hassinger, E., Malone, L., Matsuda, T.D., & Flouquet, J. High-Field Fermi Surface Properties in the Low-Carrier Heavy-Fermion Compound URu_2Si_2. *J. Phys. Soc. Jpn.* **81**, 074715 (2012).

[57] Pourret, A., Palacio-Morales, A., Krämer, S., Malone, L., Nardone, M., Aoki, D., Knebel, G., & Flouquet, J. Fermi Surface Reconstruction inside the Hidden Order Phase of URu_2Si_2 Probed by Thermoelectric Measurements. *J. Phys. Soc. Jpn.* **82**, 034706 (2013).

[58] Flouquet, J., Aoki, D., Bourdarot, F., Hardy, F., Hassinger, E., Knebel, G., Matsuda, T.D., Meingast, C., Paulsen, C., & Taufour, V. Trends in Heavy Fermion Matter. *J. Phys.: Conf. Ser.* **273**, 012001 (2011).

[59] Villaume, A., Bourdarot, F., Hassinger, E., Raymond, S., Taufour, V., Aoki, D., & Flouquet, J. Signature of hidden order in heavy fermion superconductor URu_2Si_2: Resonance at the wave vector Q_0=(1,0,0). *Phys. Rev. B* **78**, 012504 (2008).

[60] Bareille, C., Boariu, F.L., Schwab, H., Lejay, P., Reinert, F., & Santander-Syro, A.F. Momentum-resolved hidden-order gap reveals symmetry breaking and origin of entropy loss in URu2Si2, *Nature Commun*. **5**, 4326 (2014).

[61] Ran, S., Wolowiec, C.T., Jeon, I., Pouse, N., Kanchanavatee, N., White, B.D., Huang, K., Martien, D., DaPron, T., Snow, D., Williamsen, M., Spagna, S., Riseborough, P.S., & Maple, M.B. Phase diagram and thermal expansion measurements on the system $URu_{2-x}Fe_xSi_2$. *Proc. Natl. Acad. Sci. U S A* **113**, 13348-13353 (2016).

[62] Levallois, J., Behnia, K., Flouquet, J., Lejay, P., & Proust, C. On the destruction of the hidden order in URu_2Si_2 by a strong magnetic field. *EPL* **85**, 27003 (2009).

[63] Mydosh, J. A., High magnetic field behavior of strongly correlated uranium-based compounds. *Adv. Phys.* **66**, 263-314 (2017).

SUPPLEMENTARY MATERIALS

Squeezing out field-induced reentrant hidden-order in URu_2Si_2

W. Knafo[1], S. Araki[2], G. Lapertot[3], D. Aoki[3,4], G. Knebel[3], D. Braithwaite[3]

[1] *LNCMI, 143 Avenue de Rangueil, 31400 Toulouse, France*

[2] *Department of Physics, Okayama University, Okayama 700-8530, Japan*

[3] *Univ. Grenoble Alpes, CEA, IRIG, PHELIQS, F-38000 Grenoble, France*

[4] *Institute for Materials Research, Tohoku University, Ibaraki 311-1313, Japan*

e-mail: william.knafo@lncmi.cnrs.fr

February 24, 2020

16:02

Figure S1 shows ρ and $\partial\rho/\partial T$ versus T data on sample #C at zero field and different pressures up to 4 GPa. The critical temperatures T_0 and T_N are extracted for $p < p^*$ and $p > p^*$, respectively, at a sharp minimum of $\partial\rho/\partial T$.

Figures S2, S3(a,b,d,e), S4(a,b,d,e), S5(a,b,d,e), and S6(a,b) present ρ and $\partial\rho/\partial H$ versus H data measured for two samples (samples #A and #B) for a large set of pressures p from 1 bar to 3.9 GPa and temperatures T from 2.2 K to 65 K. These data were used to extract the phase diagrams shown in Figures S3(c,f), S4(c,f), S5(c,f), and S6(c).We note that, for sample #A, the measurements at ambient pressure were done using different electric contacts than the measurements under pressure. Below we describe how the different boundaries have been extracted.

At ambient pressure, we identify the low-temperature boundary H_0 of the HO phase at a sharp maximum in $\partial\rho/\partial H$ preceding the anomalies at H_1, H_2, and H_3 [see Figures S2(a-b) and S3(a-b)]. At the lowest temperatures investigated here, this maximum is decoupled from the minimum in $\partial\rho/\partial H$ at H_1. It subsists up to T = 6 K, where the anomaly at H_1 has vanished. We note that, due to higher noise, this low-temperature decoupling of H_0 and H_1 was not observed in our previous resistivity studies [45],[52]. Figure S3 (c) shows that the SDW phase is a well-defined dome separated from the hidden-order phase, in agreement with a proposition made in Ref. [63]. At temperatures $T \geq 10$ K, the anomaly at H_0 turns into a minimum in $\partial\rho/\partial H$, which is observed up to the temperature T_0 = 17.5 K, above which the hidden-order phase is destroyed.

At p = 1 GPa, the HO and AF boundaries are decoupled and anomalies in $\partial\rho/\partial H$ at $T \leq 17$ K are observed at H_0: by continuity with the ambient pressure data, we identify H_0 at a kink in $\partial\rho/\partial H$ at low-temperatures, which is replaced by a sharp minimum in $\partial\rho/\partial H$ at higher temperatures. At p = 3.6 and 3.9 GPa, the ground state is AF, there is no HO phase at zero-field, and anomalies in $\partial\rho/\partial H$ at $T \leq 21$ and 24 K, respectively, are associated with H_c:

we identify H_c at the mid-step in $\partial\rho/\partial H$ at low-temperatures, which is replaced by a sharp minimum in $\partial\rho/\partial H$ at higher temperatures. At the intermediate pressures p = 2.1 and 2.9 GPa, a field-induced decoupling of the HO boundary H_0 and the AF boundary H_c is expected from previous experiments [40]. However, at temperatures $T \geq 10$ K both transitions at H_0 and H_c induce a sharp and negative peak in $\partial\rho/\partial H$ and we cannot distinguish them (for this reason the characteristic fields of these anomalies are denoted by $H_{0,c}$ in Figure S2). As shown in Figure S3, anomalies are observed at H_0, H_2 and H_3, but not at H_1, in the resistivity of sample #B at p = 0.6 GPa. A signature of the upper boundary H_3 of the SDW phase is observed at $p = 1$ GPa, and no indication for a spin-density wave phase is found for $p \geq 2.1$ GPa. Since we could not observe the antiferromagnetism-to-HO boundary H_c under pressures $p < p_x$, H_c data from Ref. [40] were used to construct the phase diagrams. As well, to offer a complete phase diagram, the superconducting boundary from Ref. [48] was added to Figure S3(c).

At the onset of the high-field PPM phase, the HO and AF critical fields H_0 and H_c were identified in our low-temperature resistivity data. However, we could not observe the low-temperature AF→HO boundary H_c nor differentiate the H_0 and H_c lines at high temperature and the H_c versus T lines plotted in Figures 4(b-d) were taken from Ref. [40] (thermal expansion).

Figures S2(b,d) highlight that the appearance of a step in $\partial\rho/\partial(\mu_0 H)$ at H_c almost coincides with the disappearance of the broad anomalies at $H_\rho^{max,LT}$ and $H_{\partial\rho/\partial H}^{min}$, a coexistence of all these anomalies being observed at p = 3.6 GPa. The crossover field $H_\rho^{max,LT}$ increases with p, and the associated maximal value of ρ decreases and is observed up to p = 3.6 GPa, before being replaced by a broad plateau at p = 3.9 GPa. This is accompanied by the disappearance of a broad minimum in $\partial\rho/\partial(\mu_0 H)$ at the field $H_{\partial\rho/\partial H}^{min}$, where the slope in $\rho(H)$ is minimal.

Figure S7 shows that the field scales H_0, $H_m(T \rightarrow 0)$, $H_\rho^{max,LT}$ and $H_{\partial\rho/\partial H}^{min}$ increase in a similar linear manner under pressure, suggesting their close relationship.

Figure S8 shows low-temperature ρ versus H data at ambient pressure from different samples: sample #A studied here, samples #1 and #2 from Refs. [45],[52], sample #R from Ref. [49] and sample #L from Ref. [62]. While the resistivity is almost sample-independent in fields $H > H_1$, a strong sample-dependence in fields $H < H_1$ is attributed to strong orbital contribution to the resistivity inside the HO phase, due to a large carrier mobility. A fall of ρ observed for all samples in fields $\mu_0 H > \mu_0 H_\rho^{max,LT} = 29$ T is attributed to a Fermi surface reconstruction inside the HO phase. A kink is observed at a lower field of $\simeq$ 25 T in sample #1 at $T = 100$ mK (and at $\simeq$ 24 T at $T = 1.4$ K), $\simeq$ 28 T in sample #2 at $T = 100$ mK (but not at $T = 1.4$ K) [45],[52], $\simeq$ 25 T in sample #R at $T = 380$ mK [49], but neither in sample #A measured here at 1.5 K nor in sample #L [62]. Such kink was initially reported by Shishido et al. and was interpreted as the signature of a Fermi surface reconstruction [53]. The large enhancement of the high-field resistivity is induced by an orbital motion of the conduction electron, and is directly related to the sample quality. Indeed, large residual-resistivity-ratio sample generally have a higher crystal quality and a higher orbital contribution to the resistivity. The reasons why different - or no - kinks are observed in the different samples are not understood yet. They could result from different electrical contact directions. Alternatively, these kinks could result from the quenching of the non-intrinsic AF moment reported at ambient pressure [17],[18], due to internal sample distortions and inhomogeneities. Further high-pressure and high-field studies on different samples of different qualities are needed to understand the kink observed in some samples at ambient pressure, but also to determine a criterion at the AF→HO boundary H_c for pressures $p > p_c$.

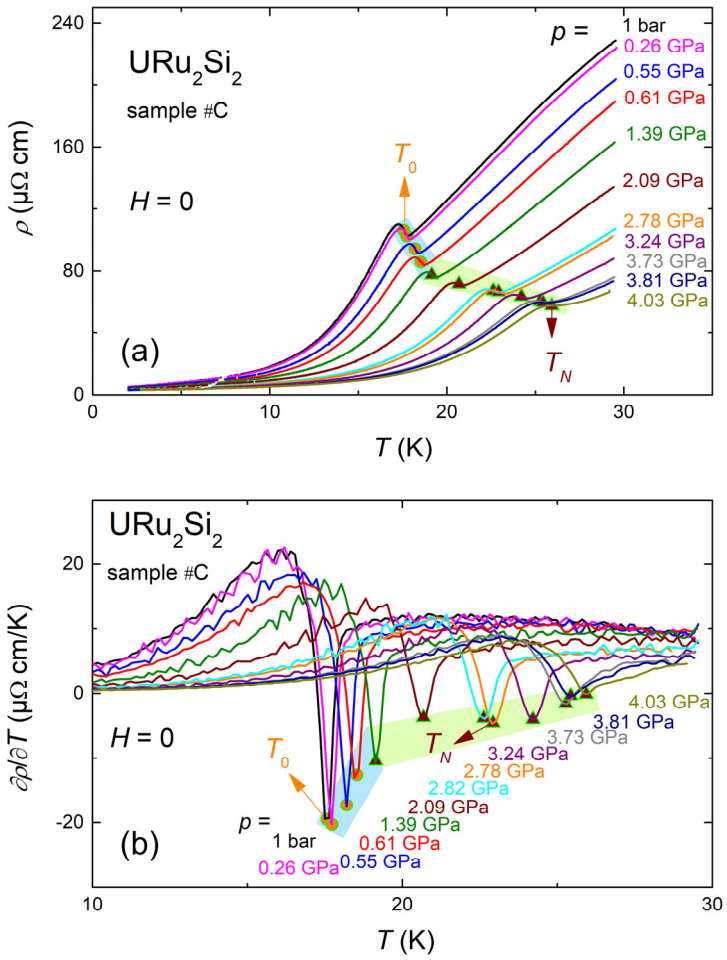

Figure S1. Zero-field resistivity ρ and its derivative $\partial\rho/\partial T$ versus temperature at different pressures of URu_2Si_2 (sample #C).

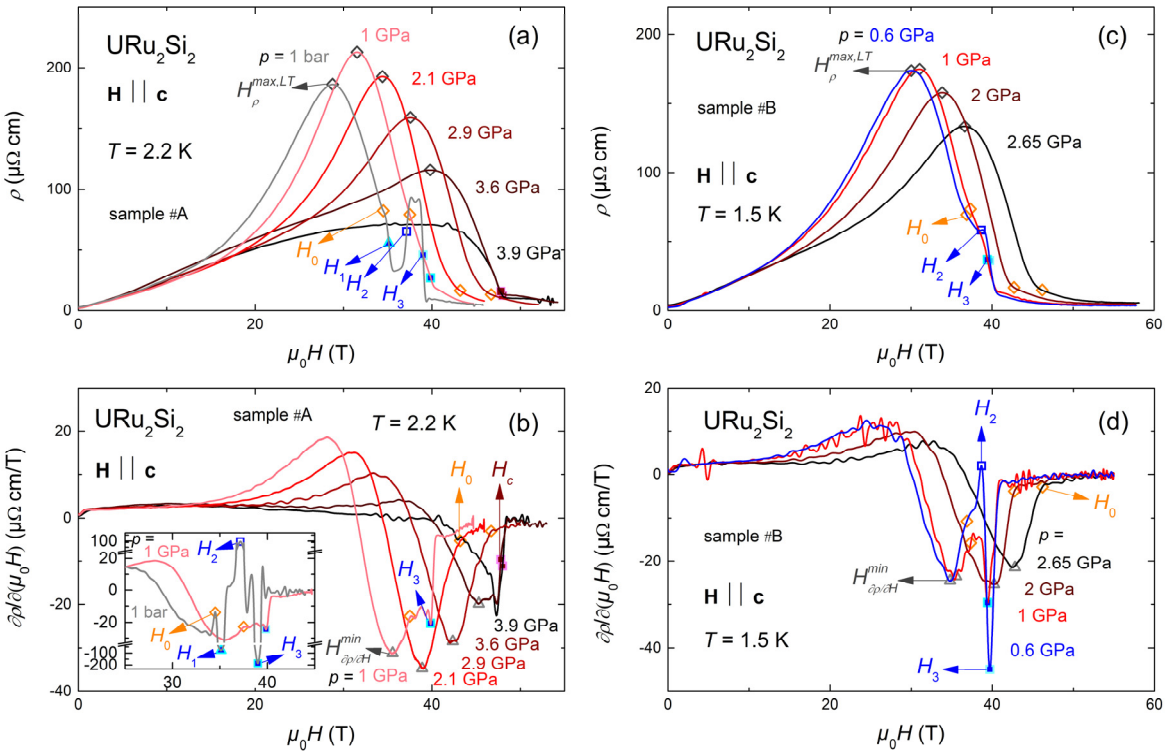

Figure S2. Low-temperature resistivity ρ and its derivative $\partial\rho/\partial H$ versus magnetic field H || c of URu_2Si_2 at different pressures. (a) ρ versus H and (b) $\partial\rho/\partial H$ versus H of sample #A at different pressures p from 1 bar to 3.9 GPa, at $T = 2.2$ K. (c) ρ versus H and (d) $\partial\rho/\partial H$ versus H of sample #B at different pressures p from 1 to 2.65 GPa, at $T = 1.5$ K.

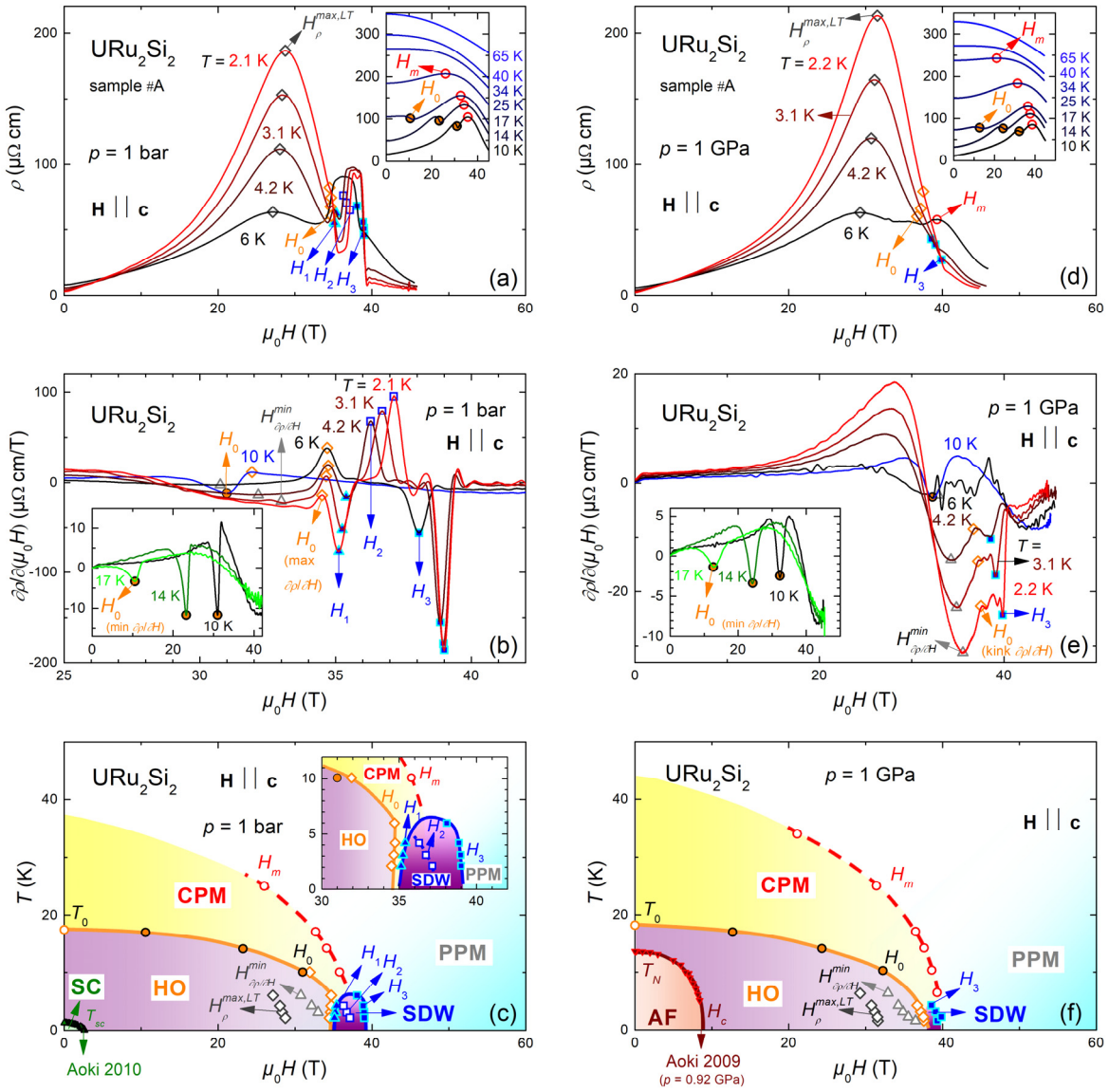

Figure S3. Resistivity ρ and its derivative $\partial\rho/\partial H$ versus magnetic field, and the resulting temperature-magnetic field phase diagrams of URu_2Si_2 (sample #A) at the pressures p = 1 bar and 1 GPa, in a magnetic field H || c. In addition to data from this work, data from Refs. [40],[48] were used to construct these phase diagrams.

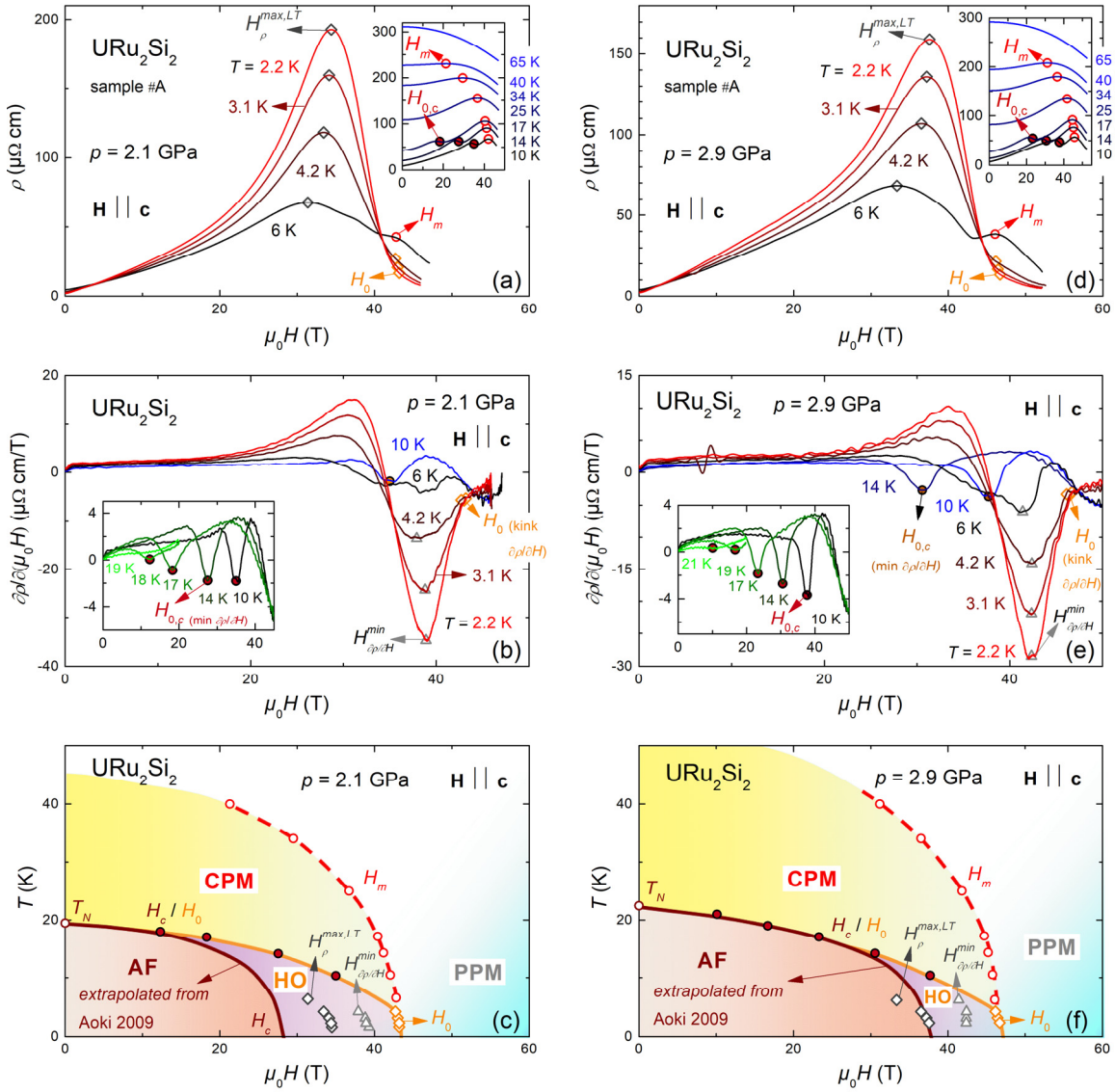

Figure S4. Resistivity ρ and its derivative $\partial\rho/\partial H$ versus magnetic field, and the resulting temperature-magnetic field phase diagrams of URu_2Si_2 (sample #A) at the pressures p = 2.1 and 2.9 GPa, in a magnetic field H || c. In addition to data from this work, data extrapolated from Ref. [40] were used to construct these phase diagrams.

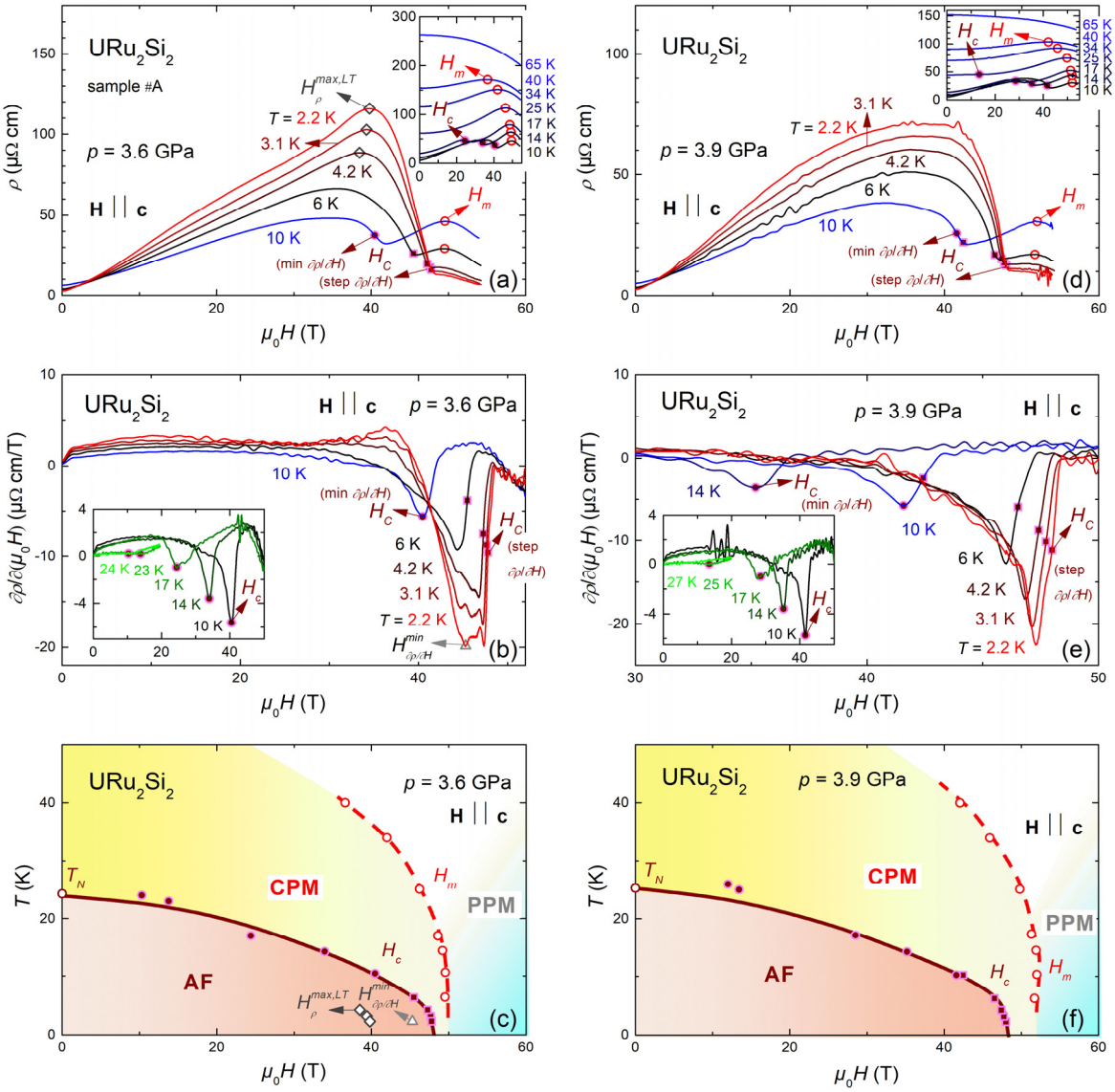

Figure S5. Resistivity ρ and its derivative $\partial\rho/\partial H$ versus magnetic field, and the resulting temperature-magnetic field phase diagrams of URu_2Si_2 (sample #A) at the pressures p = 3.6 and 3.9 GPa, in a magnetic field H || c.

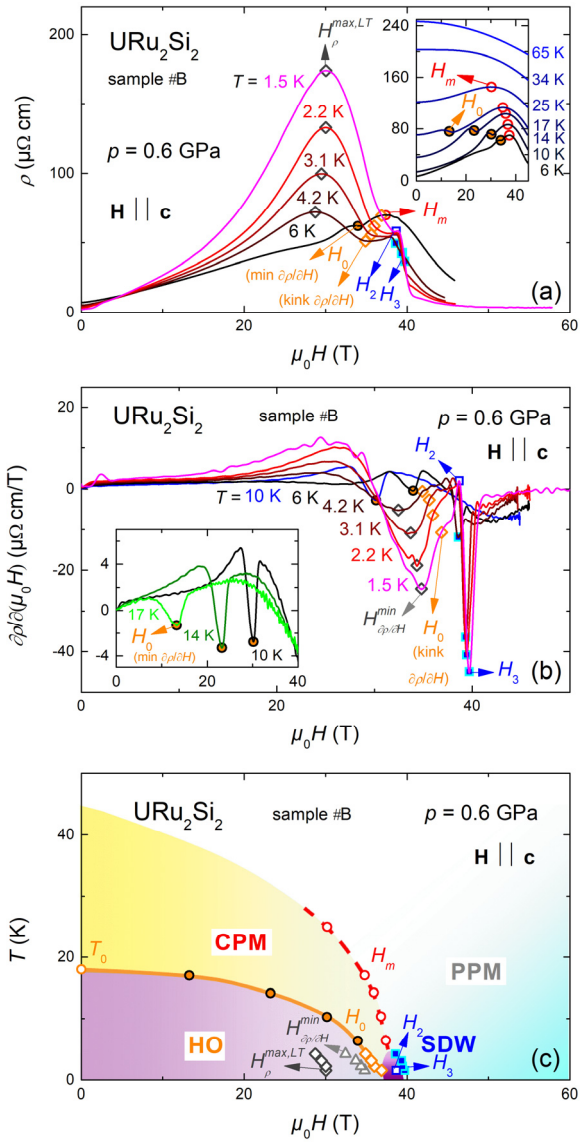

Figure S6. Resistivity ρ, its derivative $\partial\rho/\partial H$ versus magnetic field, and the resulting temperature-magnetic field phase diagrams of URu_2Si_2 (sample #B) at p = 0.6 GPa, in a magnetic field H || c.

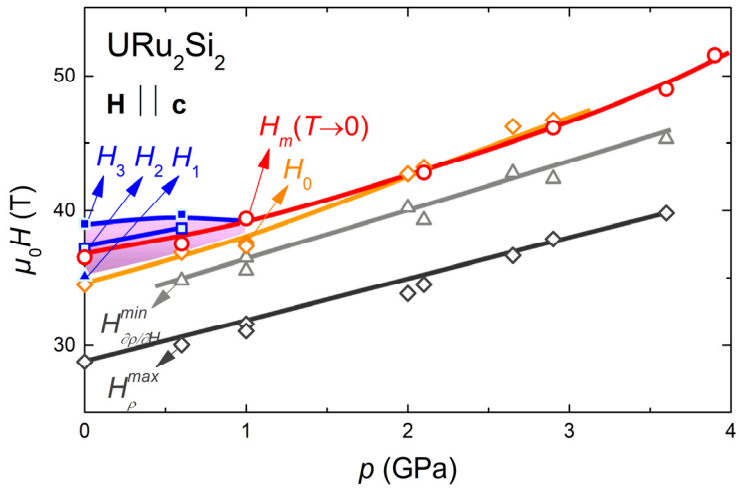

Figure S7. **Pressure dependence of selected characteristic fields.**

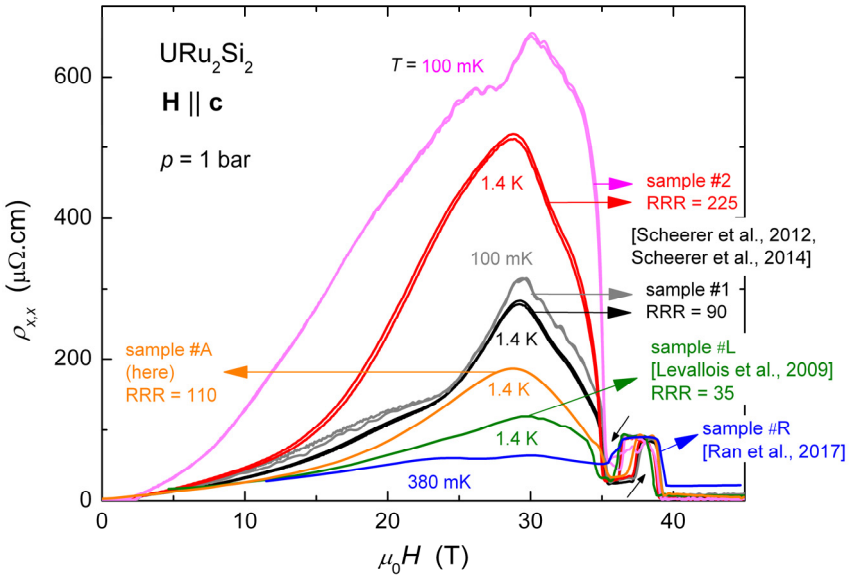

Figure S8. Resistivity ρ versus magnetic field of different samples of URu_2Si_2 at low-temperature and in a magnetic field H || c. In addition to data from this work, this graph includes data from Refs. [45],[49],[52], [62].